Biochimica et Biophysica Acta 1847 (2015) 1560–1573

Contents lists available at ScienceDirect

Biochimica et Biophysica Acta

journal homepage: www.elsevier.com/locate/bbabio

Partition, orientation and mobility of ubiquinones in a lipid bilayer

Vanesa Viviana Galassi, Guilherme Menegon Arantes *

Department of Biochemistry, Instituto de Química, Universidade de São Paulo, Av. Prof. Lineu Prestes 748, 05508-900, São Paulo, SP, Brazil

ARTICLE INFO

Article history:
Received 19 May 2015
Received in revised form 2 July 2015
Accepted 4 August 2015
Available online 6 August 2015

Keywords:
Membrane localization
Membrane insertion
Computer simulation
Free-energy profile
Molecular dynamics
Force-field parametrization

ABSTRACT

Ubiquinone is the universal mobile charge carrier involved in biological electron transfer processes. Its redox properties and biological function depend on the molecular partition and lateral diffusion over biological membranes. However, ubiquinone localization and dynamics within lipid bilayers are long debated and still uncertain. Here we present molecular dynamics simulations of several ubiquinone homologs with variable isoprenoid tail lengths complexed to phosphatidylcholine bilayers. Initially, a new force-field parametrization for ubiquinone is derived from and compared to high level quantum chemical data. Free energy profiles for ubiquinone insertion in the lipid bilayer are obtained with the new force-field. The profiles allow for the determination of the equilibrium location of ubiquinone in the membrane as well as for the validation of the simulation model by direct comparison with experimental partition coefficients. A detailed analysis of structural properties and interactions shows that the ubiquinone polar head group is localized at the water–bilayer interface at the same depth of the lipid glycerol groups and oriented normal to the membrane plane. Both the localization and orientation of ubiquinone head groups do not change significantly when increasing the number of isoprenoid units. The isoprenoid tail is extended and packed with the lipid acyl chains. For ubiquinones with long tails, the terminal isoprenoid units have high flexibility. Calculated ubiquinone diffusion coefficients are similar to that found for the phosphatidylcholine lipid. These results may have further implications for the mechanisms of ubiquinone transport and binding to respiratory and photosynthetic protein complexes.

© 2015 Elsevier B.V. All rights reserved.

1. Introduction

Ubiquinone or coenzyme-Q was described over five decades ago as a central molecule in cellular respiration and photosynthesis [1,2]. It is the ubiquitous mobile charge carrier linking distant redox centers in biological electron transfer chains. Ubiquinone receives electrons from NADH:ubiquinone reductase (respiratory complex I), succinate:ubiquinone reductase (complex II) in bacteria or mitochondria and reaction centers in purple and cyanobacteria. Cytochrome bc_1 (complex III) and the related cytochrome bf_6 then oxidize ubiquinol, the reduced counterpart of ubiquinone, to continue the electron transfer chain. Biological membranes harboring the proteins involved in bio-energetical processes contain a pool of ubiquinone and ubiquinol molecules which is responsible for 95% of the energy transduction in aerobic organisms [3–5].

Ubiquinone is an amphipathic molecule formed by a modified benzoquinone polar head and a lipid tail composed of 6 to 10 isoprenoid units in biologically relevant homologs [6,3]. The quinone head may be reduced by up to two electrons and receive two protons, passing through a semi-quinone intermediate up to the quinol form. Ubiquinone redox properties and biological function as charge carriers will depend on its partition and diffusion over biological membranes. But, despite much experimental progress obtained during the last decades, the localization and orientation of ubiquinones in biological membranes are still under heavy debate [6–15].

It has been proposed that the polar head of ubiquinones with more than 3 isoprenoid units are fully embedded in the membrane core and oriented parallel to the interfacial plane, lying in the bilayer midplane space [6–10]. Other authors have suggested that the quinone head is located close to the phospholipid polar groups and oriented parallel to its hydrocarbon tails, with the isoprenoid chain spanning the membrane [11–15]. Other proposals include the formation of ubiquinone aggregates or the partition between separate pools inside the lipid bilayer [14,16].

There is also a lack of consensus on the dynamical properties of ubiquinone embedded in lipid bilayers [17–21] as diffusion constants experimentally determined range from 10^{-9} up to 10^{-6} cm^2 s^{-1}. This high variation is due to the application of various measurement techniques [22,19] and to the usage of probes (fluorescent, spin labels, etc.) attached to ubiquinone which will alter its intrinsic diffusion properties. Nevertheless, it has been suggested that ubiquinone diffusion between respiratory complexes is the rate limiting step in the whole mitochondrial electron transfer chain [17].

* Corresponding author.
E-mail address: garantes@iq.usp.br (G.M. Arantes).

http://dx.doi.org/10.1016/j.bbabio.2015.08.001
0005-2728/© 2015 Elsevier B.V. All rights reserved.

Computer simulations can give detailed information on the partition, orientation and mobility of solutes embedded in lipid bilayers [23–25]. The accuracy and precision of the results obtained in a simulation will depend both on the energy description – the molecular mechanics (MM) force-field – and on appropriate sampling of the relevant degrees of freedom. Although there are a few simulation studies focusing on ubiquinone properties when bound to proteins [26–29], to our knowledge there is only one simulation study of ubiquinone complexed to a lipid bilayer [22,30]. Unfortunately, this study reports a very short simulation time (less than 20 ns in aggregate) which is not enough to reach equilibration and proper sampling.

Here we apply long molecular dynamics (MD) simulations and free energy calculations to investigate the properties of several ubiquinone homologs bound to model lipid bilayers. Although ubiquinone force-fields were previously available [26,28], we have tested their performance both in comparison to quantum chemical reference properties and to experimental data and judged necessary to build a new parametrization for ubiquinone compatible with the CHARMM force-field [31,32]. This energy function has been carefully validated for a series of lipids [33], including 1-palmitoyl-2-oleoyl-sn-glycero-3-phosphocholine (POPC) which was used here to build a model bilayer. We find that the polarity and flexibility of isoprenoid units should be carefully calibrated in order to obtain an accurate description for ubiquinone partition in membranes. The insertion process is simulated with enhanced sampling of several degrees of freedom that may be relevant to the interaction of ubiquinone with the bilayer. After validation of the simulations by comparison to available experimental measurements, we present a detailed analysis of the simulation results providing interesting points for the ubiquinone localization, interactions and lateral mobility when embedded in a POPC bilayer.

2. Materials & methods

2.1. Reference set and force-field parameterization strategy

A detailed parametrization for ubiquinone was performed here in accordance with the CHARMM force-field [31,32]. Details are given below for the ab initio electronic structure calculations used to build the training and test sets, and for the fitting strategy used to adjust the parameters. Ubiquinone-1 (UQ1 or UQ*n*, for *n* isoprenoid units), ubiquinol-1 (UQ1H2) and 3-methyl-3-hexene (isoprene or ISP) were used here as molecular fragments for the force-field parametrization. Please refer to Fig. 1 for atom naming used throughout the text. An equivalent naming scheme is used for ketonic ubiquinone. Isoprene was used to adjust parameters for the isoprenoid tail, whereas UQ1 and UQ1H2 were used for the quinone head.

A reference set of ubiquinone interaction energies, bond torsion potentials and molecular dipoles was built from quantum chemical (QC) calculations and used as targets for the force-field parametrization. QC calculations were conducted with GAUSSIAN 09 (Rev. A01) [34] for molecules and complexes in the gas phase. All geometry optimizations were performed with the B3LYP functional [35] and the 6–31+G** basis set [36]. All single-point energies and quantum mechanical dipole moments used in the reference set were calculated at the MP2/6-311+G(2df,2p) level [37].

Hydrogen-bonded ubiquinone–water complexes were used to model solvent interactions. Three different orientations were used for ubiquinone with oxygens O4, O1 and O3 (equivalent to O2) accepting the water hydrogen and two orientations were used with oxygen in ubiquinol (O4 and O1) donating a hydrogen to water. Hydrophobic contacts were modeled by complexes between UQ1 and methane and a ISP dimer. Interaction energies (E_i in Eq. (1)) were computed with a counterpoise scheme to correct for the basis-set superposition error [38]. The distance and orientation of all complexes were optimized whereas internal coordinates of each molecule were kept frozen at their isolated geometry. Water internal coordinates were kept frozen at the TIP3P [39] equilibrium geometry. Please refer to the Results (Fig. 2) and Supporting Information (SI, Fig. S1) for the relative orientation of the dimer complexes.

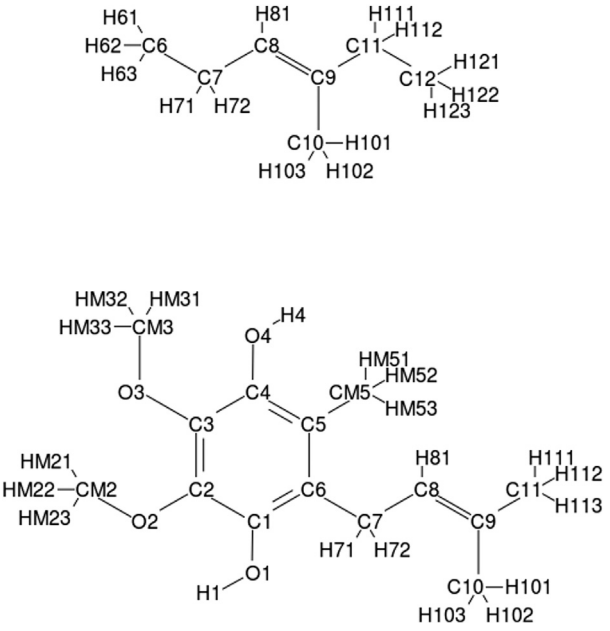

Fig. 1. Structure and atom naming of isoprene (ISP) and ubiquinol-1 (UQ1H2).

Torsions around bonds O2–C2, C6–C7 in UQ1, O1–C1, O2–C2, O4–C4 in UQ1H2, and C7–C8 and C9–C11 in ISP were evaluated (Figs. 3 and S2). Torsion potentials (E_t in Eq. (1)) were scanned in 15° or 30° angle increments by partial geometry optimizations with fixed bond lengths but flexible angle and dihedrals to avoid clashes and obtain torsional profiles representative of configurations visited at normal thermal energies. Torsions were further divided into polar (*tp*) and non-polar (*tnp*). Torsion rotamers were selected for the calculation of molecular dipoles (D in Eq. (1)).

The following error function was minimized by adjusting the force-field parameters:

$$P = \sum_i^{N_{int}} w_i \sum_j^{N_{sp}^{int}} \left| \frac{E_{i,j}^{MM} - E_{i,j}^{QC}}{E_{i,j}^{QC}} \right| + \sum_t^{N_{tp}} w_{tp} \sum_j^{N_{sp}^{tp}} \left| \frac{E_{t,j}^{MM} - E_{t,j}^{QC}}{E_{t,j}^{QC}} \right| + \sum_t^{N_{tnp}} w_{tnp} \sum_j^{N_{sp}^{tnp}} \left| \frac{E_{t,j}^{MM} - E_{t,j}^{QC}}{E_{t,j}^{QC}} \right| + w_D \sum_j^{N_{sp}^{D}} \sum_{\alpha=x,y,z} \left| \frac{D_{j,\alpha}^{MM} - D_{j,\alpha}^{QC}}{D_{j,\alpha}^{QC}} \right| \quad (1)$$

where w are the weights assigned to each property, $N_{int} = 5$ is the number of interaction pair complexes (3 hydrogen-bonded and 2 hydrophobic), and $N_{tp} = 3$ and $N_{tnp} = 4$ are the number of polar and non-polar bond torsions included in the training set. N_{sp} geometries were used for each property: $N_{sp}^{int} = 3$, including the minima and two adjacent points along the interaction profile; N_{sp}^{tp} and N_{sp}^{tnp} were either 6 or 12, depending on the angle increments, and $N_{sp}^{D} = 2$, 4 and 4 conformations respectively for UQ1, UQ1H2 and ISP. Superscripts *MM* and *QC* indicate the calculation method.

In order to obtain parameters for ubiquinone compatible with the CHARMM force-field, atom types were assigned by chemical analogy with previously parametrized molecules (Table S1). Bond and valence angle parameters were kept from the standard CHARMM values. Improper dihedrals were not included in aromatic rings or unsaturated bonds as they were not necessary to maintain planarity. Root mean square deviations of Cartesian coordinates are smaller than 0.01 nm for UQ1 geometries optimized with the force-field parametrized here in comparison to geometries optimized with the reference QC method.

Partial charges were adjusted for atoms C2/C3, O2/O3, CM2/CM3, CM5, C6, ketonic groups of UQ1 (C1/C4 and O1/O4) or phenolic groups of UQ1H2 (C1/C4, O1/O4 and H1/H4), and for isoprene C9, C10 and C11 (Fig. 1). Groups with neutral total charge were defined among the following bound atom sets: (C2, O2, CM2, HM2) and the equivalent CM3 methoxide group, (C6, C5, CM5, HM5), (C9, C10, H10, C11, H11), (C1, O1) and (C4, O4) in quinones and (C1, O1, H1) and (C4, O4, H4) in quinols. Charges for atoms in the aromatic ring and its substituents were made symmetric. Charges for isoprenoid tails longer than found in UQ1 were adapted accordingly. Partial charges for all other atom types such as aliphatic hydrogens were kept in their standard CHARMM values.

Bond torsions were fitted by altering the number of expansion terms of order n, their phase δ and force constant K_ϕ (Table S3) in the corresponding Fourier dihedral terms [31]. For ISP, torsions around bonds C7–C8 and C9–C11 were adjusted. For UQ1, polar torsion C2–O2 (and the equivalent C3–O3)and non-polar torsions C6–C7 and C7–C8 and for UQ1H2 polar torsions C1–O1 and C4–O4 were optimized.

Partial charges were optimized first by setting $w_i = 1, w_D = 1, w_{tp} = 0.04$ and $w_{tnp} = 0$ and minimizing Eq. (1). Then, dihedral parameters were optimized by setting $w_i = 1$, $w_D = 0$, $w_{tp} = 0.01$–1.0 and $w_{tnp} = 1$. After these two optimization cycles, torsions around bonds C6–C7 and C2–O2 (and the equivalent C3–O3) were still not described satisfactorily. Then, the R_{min} Lennard-Jones parameter for atoms C8, CM5, O2, O3, CM2 and CM3 were slightly changed by evaluating only the error of these three torsions. A final optimization cycle was performed by including the full training set and varying all partial charges and dihedral parameters at the same time.

All MM energies and properties used in the force-field parametrization were obtained using GROMACS package version 4.6.1 [40]. For the parameter optimization, a combination of genetic algorithm and simplex was used as described before [41]. See Tables S1, S2 and S3 for the final optimized parameter values. GROMACS compatible topologies are available upon request from the authors.

2.2. System setup and molecular dynamics simulations

The force-field obtained was tested by molecular dynamics simulations and free energy calculations. All MD simulations reported here were carried out with GROMACS package version 4.6.7 [40]. Lipid parameters were taken from the CHARMM36 force-field [33] and water was described by TIP3P [39]. The NPT ensemble was used and temperature kept at 310 K with the Bussi thermostat [42] and a coupling constant of 0.1 ps with two separate coupling groups (water and everything else). Pressure was kept at 1.0 bar with the Berendsen barostat [43] with a coupling constant of 1 ps and a compressibility of $1.0 \cdot 10^{-5}$ bar^{-1} for the unrestrained simulations and of $0.5 \cdot 10^{-5}$ bar^{-1} for the restrained free energy simulations. Semi-isotropic coupling in the direction normal to the bilayer was applied in the lipid simulations. Electrostatic interactions were handled by the particle mesh Ewald method [44] with a real space cutoff of 1.0 nm, grid spacing of 0.13 nm and quartic interpolation. All bonds were constrained using the LINCS algorithm [45] and van der Waals interactions were truncated at 1.0 nm. No dispersion corrections were applied in order to avoid artifacts in mean area per lipid and bilayer thickness [46]. The integration time step was set to 2 fs and the nonbonded list was updated every 20 fs.

Symmetric lipid bilayers containing different numbers of POPC and water molecules were built: 128 lipids and ~7900 water molecules (large system, LS), 72 lipids and ~6100 water molecules (medium system, MS) and 50 lipids and ~3300 water molecules (small system, SS). NaCl was added up to a final concentration of 0.150 M. After energy minimization using the conjugate gradient algorithm, an equilibration MD was run for 30 ns for the SS and up to 200 ns for the LS, resulting in a mean area per molecule of 0.63, 0.61 and 0.62 nm^2 respectively for the small, medium and large systems. This is in reasonable agreement with the experimental value of 0.68 nm^2[47]. The calculated bilayer thickness was 3.9 nm in all systems which is near the experimental value of 3.7 nm [47]. Mean area was computed as the ratio between the area of the membrane plane and the number of lipids per leaflet. Membrane thickness was calculated as the distance between the peaks of the lipid headgroup electron density.

Ubiquinone was inserted in the membranes using two different protocols: For the insertion of UQ1 in the LS bilayer, a pulling from the water phase towards the membrane center of mass (COM) was conducted in the membrane normal direction with the pull code in GROMACS and a rate of 4.10^{-5} nm ps^{-1}. For all other insertions, the protocol described by Javanainen was used [48]. In short, ubiquinone was placed at the membrane edge using a visualization tool, the box dimensions were increased accordingly, water and lipids were restrained in the membrane normal direction to avoid escaping to the empty space generated, and a 5 ns MD simulation was run with an anisotropic barostat and a reference pressure of 1000 bar in the direction which ubiquinone was placed. After ubiquinone was immersed into the membrane, the system was relaxed by removing all restrains and the pressure reversed back to semi-isotropic and 1.0 bar in another 30 ns MD run. The mean area and bilayer thickness were monitored to check for equilibration.

Ubiquinone concentration in percentage per mole was 0.8% in LS, 1.4% in MS and 2.0% in SS membranes. This is similar to previous ubiquinone simulations [22] and to the physiological concentration range of 1–3% [8].

Unconstrained MD simulations were performed for the embedded ubiquinones using the last frame from the umbrella sampling window with minimum free energy (see below). Trajectories with 200 ns were collected for UQ1, UQ1H2 and UQ2 and trajectories with 400 ns were collected for UQ6 and UQ10. Two simulations starting from different isoprenoid tail conformations (folded and fully extended) were performed for UQ10 with the quinone head positioned near the minimum free energy configuration found for the other ubiquinones. All properties calculated from these two simulations are equivalent and, hence, independent of the tail starting conformation.

Diffusion coefficients were calculated from the linear phase of the mean squared displacements with dimensionality set to 2, as only lateral diffusion along the membrane plane was processed [49]. The orientation of the ubiquinone head was calculated from the angle formed between the quinone ring plane (defined by atoms C1, C3 and C5) and the bilayer midplane. Flexibility and extension of the isoprenoid tail were evaluated from the distance between the last carbon of the tail (CT) and both the quinone head COM and the bilayer midplane. Contacts between ubiquinone atoms and different groups in POPC were defined with a 0.3 nm cut-off. Order parameters S_{CD} for lipid methylene units were calculated using the program LOOS [50].

2.3. Free energy calculations

Umbrella sampling (US) [51] and bias-exchange metadynamics (BEMD) [52] were used to compute the free energy profile for ubiquinone insertion into the model bilayers. The distance between the ubiquinone head COM and the membrane COM along its normal z-axis was used as the insertion reaction coordinate.

Initial configurations for each US window were extracted from a non-equilibrium trajectory generated with an extra pulling force acting over ubiquinone along the z-axis in the range [0,5] nm for the POPC bilayer (Section 2.2). The pulling spring constant was 300 kJ mol^{-1} nm^{-1} and the pulling rate was 4.10^{-5} nm ps^{-1}. US windows were chosen equally spaced by 0.125 nm in the range z = [0.00,2.75] nm while ubiquinone is inside the membrane or in the interface and by 0.250 nm in the range z = [3.0,5.0] nm while ubiquinone is in water. The umbrella potential was set with k_{umb} = 1000 kJ mol^{-1} nm^{-1} in the membrane range and with k_{umb} = 500 kJ mol^{-1} nm^{-1} in the water range.

Simulations run for 60 ns in each US window with a total aggregate time of 5.5 μs for all US simulations. The reaction coordinate was recorded each 200 fs. Potentials of mean-force (PMF) were calculated from the reaction coordinate occurrence using the weighted histogram analysis method [53]. The PMFs shown were obtained from 30 ns of equilibration and 30 ns of accumulation in each window. PMF uncertainties were estimated by bootstrap analysis using the Bayesian method [54]. It should be noted that ubiquinone insertion in the US simulations was carried out over only one bilayer leaflet (z-axis > 0).

The bias-exchange metadynamics method [52] was applied to enhance sampling along degrees of freedom orthogonal to the insertion reaction coordinate. BEMD is an extension of metadynamics [55] for replica exchange in a collective variable (CV) space. The PLUMED plug-in version 2.1 [56] was used for these simulations.

The following CVs were chosen besides the z-axis coordinate: C6–C7 bond torsion which was identified with a high torsional barrier (Fig. 3); the angle formed between ubiquinone atoms C1and C4 and the COM of the membrane (θ_{UQ}). Following a recent publication that studied the insertion of ethanol in a model bilayer with BEMD simulations [24], coordination numbers N between ubiquinone and membrane lipid tails or water molecules were also included as CVs. These contacts were calculated with the soft function:

$$N_{g_1-g_2} = \sum_{i\in g_1}\sum_{j\in g_2}\frac{1-\left(\frac{r_{ij}}{r_0}\right)^n}{1-\left(\frac{r_{ij}}{r_0}\right)^m} \tag{2}$$

where r_{ij} is the distance between atoms i and j and the sums run over two sets of atoms (g_1 and g_2). Values of $r_0 = 0.3$ nm, $m = 12$, and $n = 6$ were adopted. Four contact number CVs (N_{g1-g2}) were defined by the combination of $g_1 = \{H,I\}$ and $g_2 = \{A,W\}$, where H indicates the set of ubiquinone head atoms, I is the set of isoprenoid tail atoms, A is the set of lipid acyl chain carbon atoms and W is the set of water oxygen atoms.

For UQ1, UQ1H2 and UQ2, BEMD simulations were performed for 120 ns with the 7 CVs defined in the previous paragraph and an extra replica without metadynamics boost. For UQ0, two BEMD simulations were performed with a different combination of CVs. One simulation was performed for 160 ns with 4 CVs: z-axis, θ_{UQ}, N_{H-A} and N_{H-W}, and another was done for 120 ns with 4 CVs: z-axis, z-axis with a slower gaussian function deposition, and torsions around C2–O2 and C3–O3 bonds. All BEMD simulations were performed in SS bilayers (Section 2.2). For UQ1, a BEMD simulation was repeated with the MS bilayer. The gaussian height for all CVs was set to 0.5 kJ mol^{-1} and gaussian widths were set to 4 nm for the coordination number CVs and to 0.2 nm for all other CVs. The frequency of gaussian deposition was set to 4 ps for the z-axis CV, 10 ps for the coordination number CVs and 20 ps for all other CVs (including the z-axis with slower deposition). Exchanges were attempted randomly among replicas every 20 ps.

PMFs were obtained from the BEMD simulations by averaging N_{BE} profiles generated at different accumulation times from the history dependent potential of the sum of gaussian functions deposited for a given CV [57,58]. Typically, 10 to 12 profiles were generated, the first 2 or 3 with the shortest accumulation times were discarded and N_{BE} ~ 8–10 profiles were averaged. For total simulation times longer than about 80 ns, the system could freely diffuse along the enhanced CV. Uncertainties were estimated from the standard deviation of the mean [57].

Standard binding free energies between ubiquinone and the lipid membrane, ΔG_b°, were determined by trapezoidal integration of the PMF profiles according to [59]:

$$e^{-\beta\Delta G_b^\circ} = \frac{\int_{bound} e^{-\beta[PMF(z)]}dz}{\int_{unbound} e^{-\beta[PMF(z)]}dz}. \tag{3}$$

A separate ΔG_b° was calculated for each leaflet in the BEMD profiles with bound regions set to $z \in [0.0,2.5]$ nm or $z \in [-2.5,0.0]$ and unbound region set to $z \in [2.5,5.0]$ nm or $z \in [-5.0,-2.5]$ nm, respectively. Results shown are an average of the two separate ΔG_b°. For the PMFs obtained from US, the bound region was set to $z < 2.6$ nm, 2.9 nm and 4.0 nm for UQ1, UQ2 and UQ6, respectively. These boundaries correspond to the z value where the PMF(z) reached a plateau. The unbound region was set such that the same integration volume was used, resulting in the calculation of a standard free energy. Uncertainties were propagated from the PMFs following standard formulas [60].

3. Results & discussion

3.1. Performance of the new CHARMM compatible parametrization

As described in Section (2.1), partial charges, Lennard-Jones parameters (R_{min}) and dihedral force constants of a CHARMM compatible force-field were adjusted in order to reproduce high-level QC data for bond torsion potentials, molecular dipoles and interaction energies of fragment molecules ubiquinone-1, ubiquinol-1 and isoprene isolated and in complex with water or apolar molecules.

The description of molecular and energetic properties was greatly improved with the force-field parametrized here, both qualitatively for the shape of bond torsion potentials or the description of hydrogen-bonded complexes, as well as quantitatively for the relative stability between rotamers or complexation energies. In particular, it was noted that the molecular dipole of the apolar isoprene molecule (ISP) was incorrectly described by up to 2 Debye using the previously available CHARMM compatible force-fields (Table S4) [26,28]. This was corrected in the current parametrization which leads to significant improvements on the bilayer partition free energy of ubiquinones.

A few examples are noted below to illustrate the performance of the available force-fields in comparison to high-level QC calculations. Please refer to SI (Figs. S1 and S2) for a complete set of results for interaction and torsion profiles used for training and testing the force-fields. This analysis may help to identify flaws in the potential energy description and suggest internal degrees of freedom which should be sampled carefully in condensed-phase simulations.

For the interaction energy profiles used in the parametrization training set (Figs. 2A and S1), deviations of the ubiquinone force-field obtained here from the QC reference are always smaller than 5 kJ/mol near minima and over longer separation distances. Differences are at most 10 kJ/mol for interaction energy profiles used only for testing such as the one in Fig. 2B. Other force-field parametrizations [28,26] show much higher deviations and even qualitatively wrong descriptions such as in a hydrogen bond between water and the quinol hydrogen (Fig. 2B).

The shapes of the potential energy profile and relative energies between minima are well described by the force-field obtained here for ubiquinone bond torsions either included or not in the parametrization (Figs. 3 and S2). Deviations smaller than 10 kJ/mol are observed near energy barriers. On the other hand, previously available MM parametrizations result in torsions with incorrect shapes (e.g., in Fig. 3A) and in high deviations near energy barriers (Fig. 3B and C).

Torsions in the isoprenoid tail around bond C($4 + 5i$)–C($6 + 5i$) in the i-th isoprenoid unit were also improved (Fig. 3A) leading to a more accurate description of ubiquinone homologs with long isoprenoid tails. The torsion around the C6–C7 bond was particularly challenging to be described with the available force-fields (Fig. 3B). During the parametrization of the dihedral force constants, it was noted that the barriers along this bond torsion could not be adjusted due to too high repulsion interactions between atoms C8 and CM5 and their respective hydrogens. Thus, Lennard-Jones parameters for both carbon atoms were changed and a significant improvement (~20 kJ/mol) was obtained. Nevertheless, the force-field parametrized here is still unable to describe the barrier near dihedral angle ~270° with an accuracy

better than 15 kJ/mol. In fact, this is the highest deviation observed over all potential energy comparisons done here. Because the C6–C7 bond torsion contributes significantly for the ubiquinone flexibility as it connects the quinone head with the isoprenoid tail, sampling along this torsion was carefully monitored in the insertion free energy calculations.

Methoxide group torsion around bond C2–O2 (or C3–O3) also shows high barriers when described with previous parametrizations (see Fig. 3C for UQ1H2 and Fig. S2 for UQ1). The barrier deviations were also due to too high repulsion interaction between CM2 (or CM3) and O1 (or O4) and were again corrected with changes in the Lennard-Jones R_{min} parameter. The deviations were greatly improved with the force-field parametrization presented here.

3.2. Free energy profiles for partition into the membrane

Potentials of mean-force (PMFs) for the insertion of various ubiquinone homologs into model POPC bilayers were calculated in order to check the accuracy of the parametrized force-fields and to determine the equilibrium ubiquinone localization along the membrane normal. Umbrella sampling and bias-exchange metadynamics were used to enhance sampling over the membrane insertion coordinate (z-axis defined above) and along orthogonal collective coordinates in the case of BEMD. In this section, we describe the PMFs and derived free energy quantities (ΔG_b°). Details of the ubiquinone localization and contacts within the bilayer are left to Section 3.3 below.

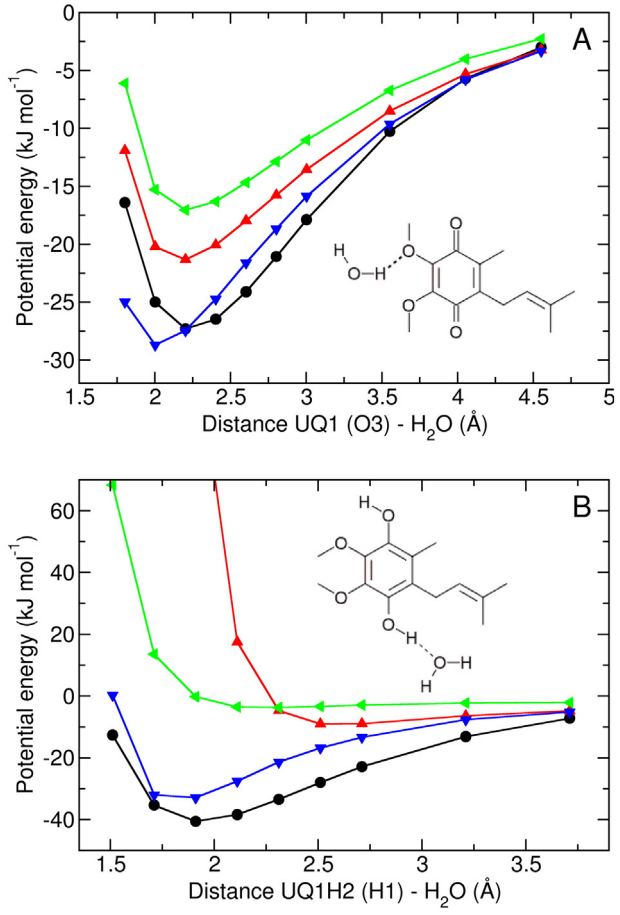

Fig. 2. Interaction energies for ubiquinone–water hydrogen-bonded complexes. QC reference energies were obtained at the MP2/6-311+G(2df,2p) level (black circles). The other curves are different ubiquinone MM parametrizations proposed by Kaszuba et al. [28] (red up triangles), Autenrieth et al. [26] (green left triangles) and here (blue down triangles). Complex orientation is shown as insets. Data in panel A was included in the force-field parametrization while panel B was used only for testing purposes.

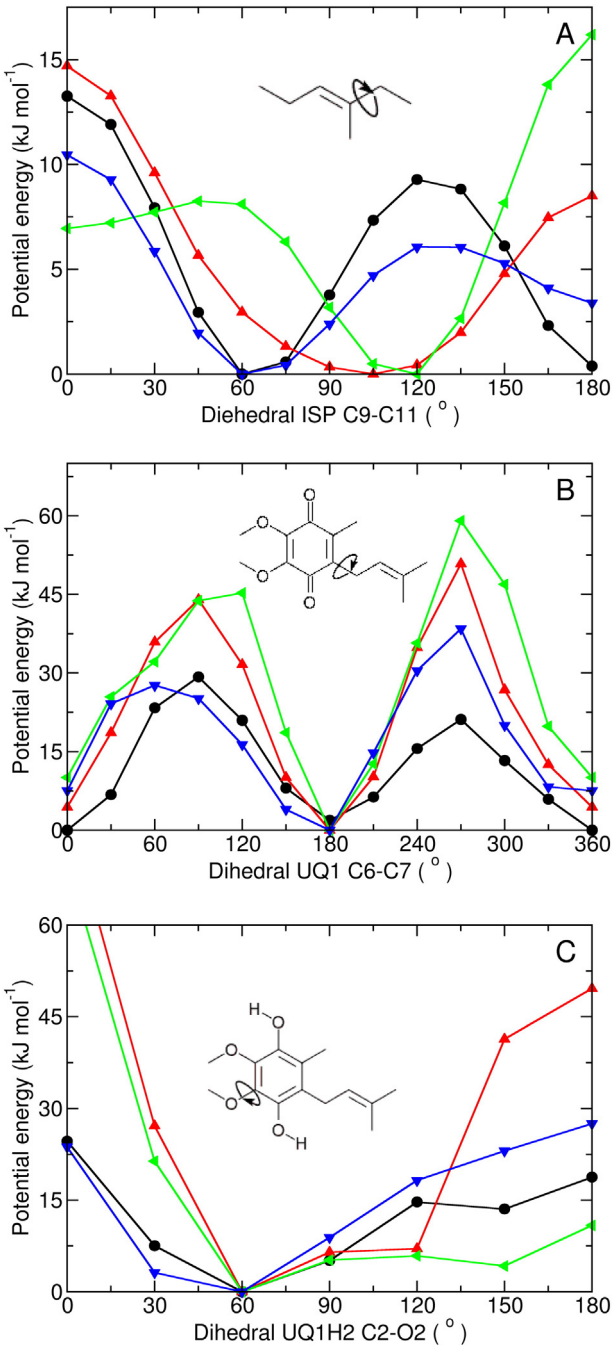

Fig. 3. Bond torsion potentials for ubiquinone obtained at QC and MM levels as indicated in the legend for Fig. 2. Data from panels A and B were included in the force-field parametrization while panel C was used only for testing.

Fig. 4 shows that the general shape and minima of the PMF obtained by US change little for the three ubiquinones tested. One isoprenoid unit is enough to partition ubiquinone UQ1 into the bilayer and, as expected, increasing the number of isoprenoid units enhances hydrophobicity and consequently membrane affinity. But, the z-axis position of the PMF minima is rather constant (1.68 nm for UQ1 to 1.55 nm for UQ6). These minima correspond to the preferential localization of the ubiquinone head in the membrane and have been observed in the same z-axis range for the insertion of other amphiphile molecules [23]. Thus, previous proposals of the ubiquinone head localization in the middle of the bilayer are not plausible [6–10,22].

The translocation of ubiquinone from one bilayer leaflet to the other will depend on the free energy barrier separating the

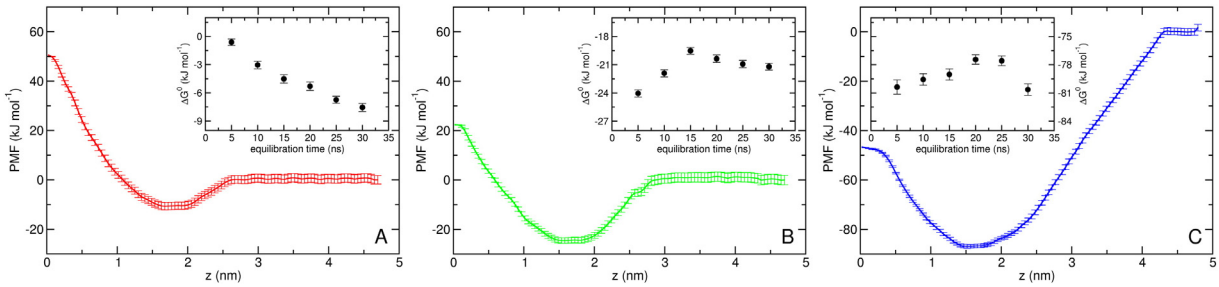

Fig. 4. PMFs for ubiquinone insertion in large (LS) POPC bilayer obtained by umbrella sampling for UQ1 (panel A), UQ2 (B), and UQ6 (C). The insets show the calculated binding free energy ΔG_b as a function of equilibration time for fixed 30 ns of accumulation time in each US window.

membrane center and the minima in the PMF. The barrier decreases from 62 ± 2 kJ mol^{-1} for UQ1, to 47 ± 2 kJ mol^{-1} for UQ2 and to 40 ± 2 kJ mol^{-1} for UQ6. This is again in line with the higher hydrophobicity of ubiquinones with longer tails and suggests that an approximate barrier of ~40 kJ mol^{-1} should be observed for the "flip-flop" of natural ubiquinones with long isoprenoid tails (UQ6–UQ10). Thus, the translocation of ubiquinone is a rare event and will not be observed faster than the micro- to milli-second time scale. This is in agreement with the flip-flop rate estimated from NMR measurements [11]. There is no significant barrier in the PMFs for the water-membrane insertion process, as also observed for the insertion of small polar and charged molecules [61,62,24] or large amphiphiles [23], suggesting that ubiquinone insertion will be diffusion-controlled. It should be noted that the lack of an insertion barrier may also be due to incomplete sampling for the ubiquinones with longer isoprenoid tails.

Although we expect to have obtained converged PMFs for UQ1 and UQ2 (see discussion below), the same cannot be said for UQ6 which has a longer tail and would require longer simulation times for convergence. It has been recently noted that the calculation of PMFs in the membrane–water interface region for the insertion of amphiphiles with long hydrophobic tails can be problematic [23]. Although errors in this region of the PMFs result in incorrect calculated binding free energies, they do not effect significantly the *z*-axis location of PMF minima nor the translocation barrier which should be well described by the PMFs shown in Fig. 4 even for UQ6. Thus, our discussion in the previous paragraph is accurate, but the value estimated below for the free energy of binding of UQ6 (Table 1) should only be considered qualitatively.

It has been noted [63,61,62,23] that the solvation substitution occurring in membrane–water interfaces is often the process with the slowest relaxation to be described during the simulation of solute insertion into lipid bilayers. In accordance, we have noticed a sudden change in the hydration number of the ubiquinone tail for homologs with two or more isoprenoid units in US windows located at the membrane–water interface. For UQ2, it was observed at $z \sim 2.8$ nm (Fig. S3), corresponding to simulation windows where the isoprenoid tail does not transition between water and bilayer and stays in only one of these phases during all accumulation time. This sudden change may also be causing the small flat region observed at similar *z* coordinate on the calculated PMF for UQ2 (Fig. 4) [23].

To enhance sampling along slow degrees of freedom such as the number of contacts of ubiquinone with water and with the lipid we

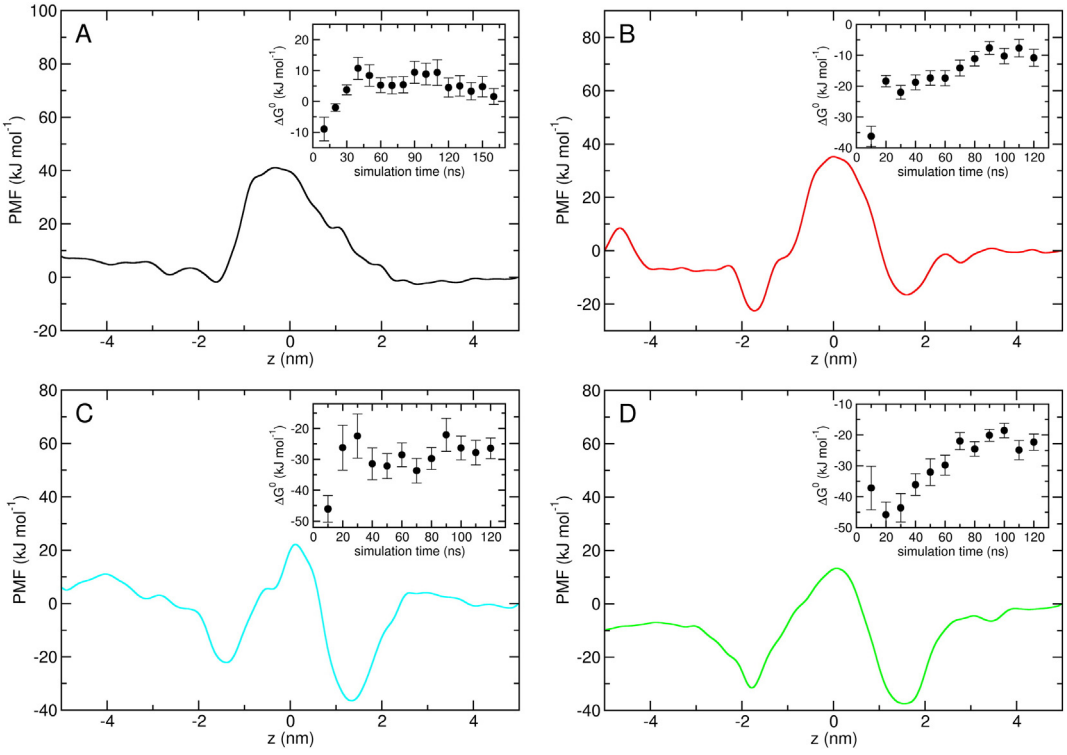

Fig. 5. PMFs for ubiquinone insertion in small (SS) POPC bilayer obtained by bias-exchange metadynamics for UQ0 (panel A), UQ1 (B), UQ1H2 (C), and UQ2 (D). The insets show the calculated binding free energy ΔG_b as a function of total simulation time.

Table 1
Experimental and calculated standard binding free energies (ΔG_b°, in kJ mol^{-1}) between ubiquinone homologs and model bilayers.[a]

	Experimental	US	BEMD
UQ0	−2[65]		2 ± 2
UQ1	−17[66], −20[18]	−8 ± 1	−11 ± 3
UQ1H2	−18[67]		−26 ± 3
UQ2	−21[18], −24[66]	−21 ± 1	−22 ± 3
UQ6		−81 ± 1	

[a] Experimental free energies were obtained from partition coefficients measured for bovine heart submitochondrial particles [66], asolectin vesicles [18,67] and water–octanol [65] mixtures assuming a temperature of 310 K. Values calculated in POPC bilayers were obtained from US and BEMD simulations employing the force-field parametrized here. Uncertainties were propagated from the corresponding PMFs.

have employed BEMD simulations. Internal bond torsions of the inserted molecule can also difficult sampling [25]. Thus, we have enhanced sampling over ubiquinone tail C6−C7 which was identified with large energy barrier (Fig. 3).

PMFs shown in Fig. 5 were obtained from the BEMD simulations for insertion over the two bilayer leaflets. The PMF shape is more rugged than the US PMFs as a result of the gaussian deposition scheme that enhances sampling along the membrane normal z-axis [24]. Nevertheless, for UQ1 and UQ2 the position of the PMF minima (~1.65 nm in modulo) and the translocation energy barrier (55 ± 10 kJ mol^{-1} for UQ1 and 47 ± 10 kJ mol^{-1} for UQ2) are equivalent to those observed in the US PMFs. It should be noted that uncertainties reported for free energies obtained by BEMD are higher than those reported for US due to higher standard deviations obtained in the averaging procedure used to calculate the PMFs from BEMD (see Materials & methods). This scheme is formally different and more likely to accumulate statistical errors than the bootstrap analysis used to estimate the uncertainties of PMFs from US.

The minima observed in the PMF for UQ0 insertion were not pronounced in either the simulation shown in Fig. 5 or in a simulation with enhanced sampling for C2–O2 and C3–O3 bond torsions (data not shown) suggesting that our UQ0 model gives a very low affinity for the membrane. Ubiquinol UQ1H2 insertion PMF and localization in the membrane are similar to the other quinone homologs. This is in agreement with their comparable experimental reactivity [64] and free energy of binding (Table 1).

The accuracy of the PMFs simulated here for ubiquinone insertion into a POPC bilayer can be accessed by comparisons of the calculated free energy of binding (ΔG_b°, Eq. (2)) with free energies derived from experimental partition coefficients as shown in Table 1. It should be noted that the available experimental data were obtained in conditions and system composition which are different from those simulated here. For instance, the partition coefficient reported for UQ0 was obtained in a water–octanol mixture [65]. For the other ubiquinones, partition coefficients were obtained in bovine heart submitochondrial particles with a mixed lipid composition [66], or in sonicated asolectin vesicles mainly composed by phosphatidylcholine [67]. Thus, part of the divergence between experimental and simulated values may be attributed to differences in the model composition.

The highest differences from experiment in the binding free energy calculations are observed for UQ1 and UQ1H2 in Table 1. For the quinone, the calculated ΔG_b° suggests an affinity of 6–12 kJ mol^{-1} lower than the experimental values. For the quinol, an affinity of 8 kJ mol^{-1} higher than experiment is found. These differences may be due to unbalanced interactions of the quinone (or quinol) head with the lipid polar group. Values calculated for UQ0 and UQ2 are almost equivalent to the experimental measurements. No experimental value for UQ6 partition coefficient is available, but the binding free energy for biological ubiquinones was estimated to be more negative than −60 kJ mol^{-1}[66]. As noted above, we do not expect to have a quantitative value for UQ6 binding free energy. Thus, given the statistical uncertainty in the simulations, the composition differences between

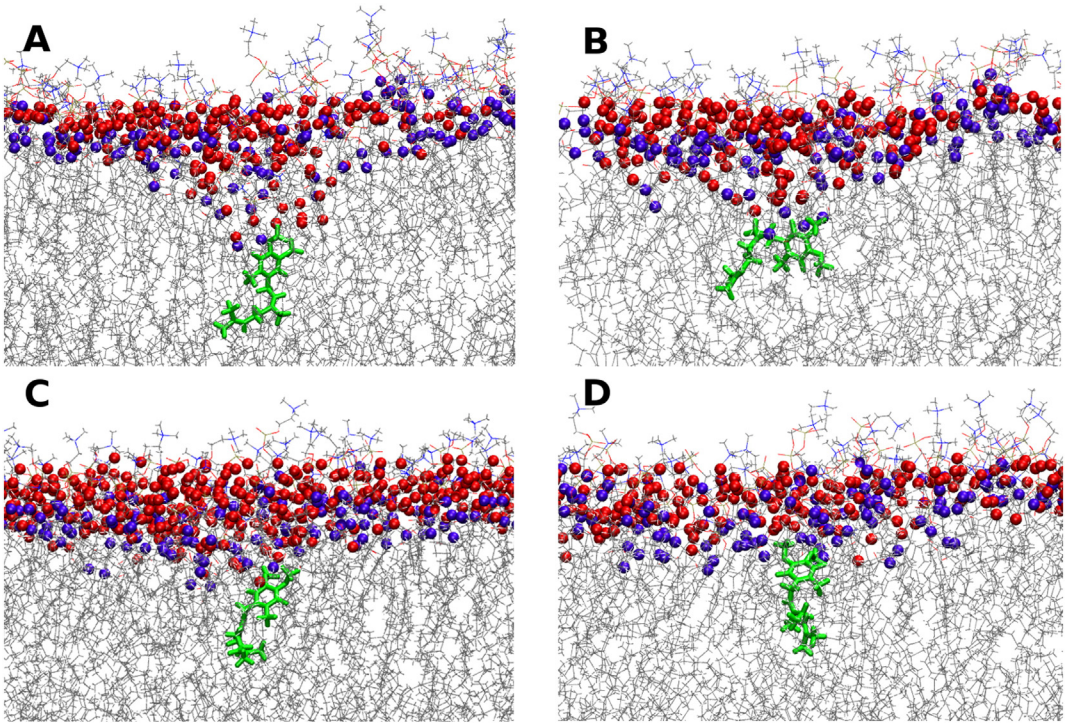

Fig. 6. Membrane protrusion upon ubiquinone insertion. Snapshots were obtained from the last frames of UQ2 simulation in US windows centered at $z = 0.2$ nm (panel A), $z = 0.4$ nm (B), $z = 0.6$ nm (C) and $z = 0.9$ nm (D). Ubiquinone is represented in green sticks. Membrane is represented in lines with lipid glycerol oxygen atoms in violet balls and interfacial water oxygens in red balls.

the simulated models and experimental setups, and the variations of measured values, we conclude that our force-field yields PMFs and derived free energy quantities in good agreement with experimental observations.

The agreement of ΔG_b° calculated for UQ1 and UQ2 between US and BEMD methods also suggests a good accuracy for the calculated PMFs. These two methods estimate free energies using different assumptions and the simulations were carried out independently in different bilayer preparations (LS for US and SS for BEMD). The influence of the bilayer size on the binding free energy calculated here from the BEMD simulation should be negligible. For instance, $\Delta G_b^\circ = -10 \pm 3$ kJ mol^{-1} for UQ1 insertion in the MS bilayer is equivalent to the value calculated for the SS bilayer (Table 1).

On the other hand, the force-field description changes the calculated biding free energy considerably. For the insertion of UQ1 in the LS membrane using US and the force-field proposed by Kaszuba et al. [28], the calculated $\Delta G_b^\circ = 1 \pm 1$ kJ mol^{-1} is 18 kJ mol^{-1} higher than the experimental value. Such high hydrophilicity of the Kaszuba et al. potential can be attributed to the incorrect high polarity of the isoprenoid tail observed with their charge parametrization (Table S4). This artifact will be more pronounced for ubiquinones with longer isoprenoid tails as the total dipole for the longer tails will be a vector sum of the contributions of each isoprenoid unit.

Convergence of the calculated PMFs can be accessed from the derived free energies of binding obtained over different equilibration (US) or total simulation (BEMD) times as shown in the insets of Figs. 4 and 5. For the US simulations, the calculated ΔG_b° shows variations smaller than ~3 kJ mol^{-1} after 15 ns of equilibration time in each window. For the BEMD simulations, ΔG_b° shows variations smaller than ~6 kJ mol^{-1} after 80 ns of total simulation time. Both variations are comparable to the uncertainties estimated from the PMFs. Higher precision would require much longer simulation times [61]. However, we do not judge a higher precision necessary as the variations of reference partition coefficients measured for same ubiquinone in different experimental preparations are similar to the present calculated statistical uncertainties (~3 kJ mol^{-1}).

Besides essential sampling over the bilayer insertion coordinate (z-axis), we identify that enhanced sampling over the coordination numbers between water or lipid molecules and the ubiquinone head and tail (N_{g1-g2} in Eq. (1)) are the most important ones in order to describe the slow relaxation of the solvation substitution process in the membrane interface. Thus, convergence of calculated PMFs in BEMD simulations can be significantly accelerated for ubiquinones with longer isoprenoid tails by enhanced sampling of the coordination between water and tail. Enhanced sampling of ubiquinone orientation and internal degrees of freedom are less important. For instance, a BEMD simulation with enhanced sampling of methoxide bonds (C2–O2 and C3–O3) resulted in a $\Delta G_b^\circ = 1 \pm 1$ kJ mol^{-1} for UQ0 which is equivalent to the binding free energy calculated for UQ0 without such enhancement (Table 1). Rotations through these methoxide bonds as well as in quinol hydroxide bonds (H1–O1 and H4–O4) are observed over the simulation time of the US and BEMD simulations (Fig. S5). It should be noted that rotations over C6–C7 bonds were not observed during the accumulation time of the US windows, but were observed on the longer free MD simulations (see Section 3.3 and the discussion of Fig. 8). However, increasing the sampling of this C6–C7 bond as done in the BEMD simulations does not lead to significant differences in the calculated PMF and derived quantities.

3.3. Ubiquinone-membrane structure and interactions

Ubiquinone insertion induced a structural perturbation in the bilayer when the ubiquinone polar head group is located near the membrane midplane (ubiquinone head COM with $z < 0.6$ nm) as shown in Fig. 6. This protrusion has a "funnel"-like shape and corresponds to both lipid head groups and water molecules dragged towards the membrane center. The number of contacts with water also reports the significant hydration of the ubiquinone head when partitioned inside the membrane (Fig. S3). The opposite effect when ubiquinone desorbs from the bilayer was not observed [61], suggesting that the solvation substitution in the bilayer interface is more favorable than membrane deformation.

Results presented over the remaining of this and the next sections (Figs. 7–12) were obtained from unconstrained MDs started from the last frame of the 60 ns US window with lowest free energy value in the respective PMF. This should correspond to the equilibrium configuration of ubiquinone embedded in the bilayer. Isoprenoid tails should be well equilibrated as restrictions in US were included only in the ubiquinone head. The last 180 ns for UQ1–UQ2 and the last 360 ns for UQ6 and UQ10 of the unconstrained MD trajectories are used for analysis.

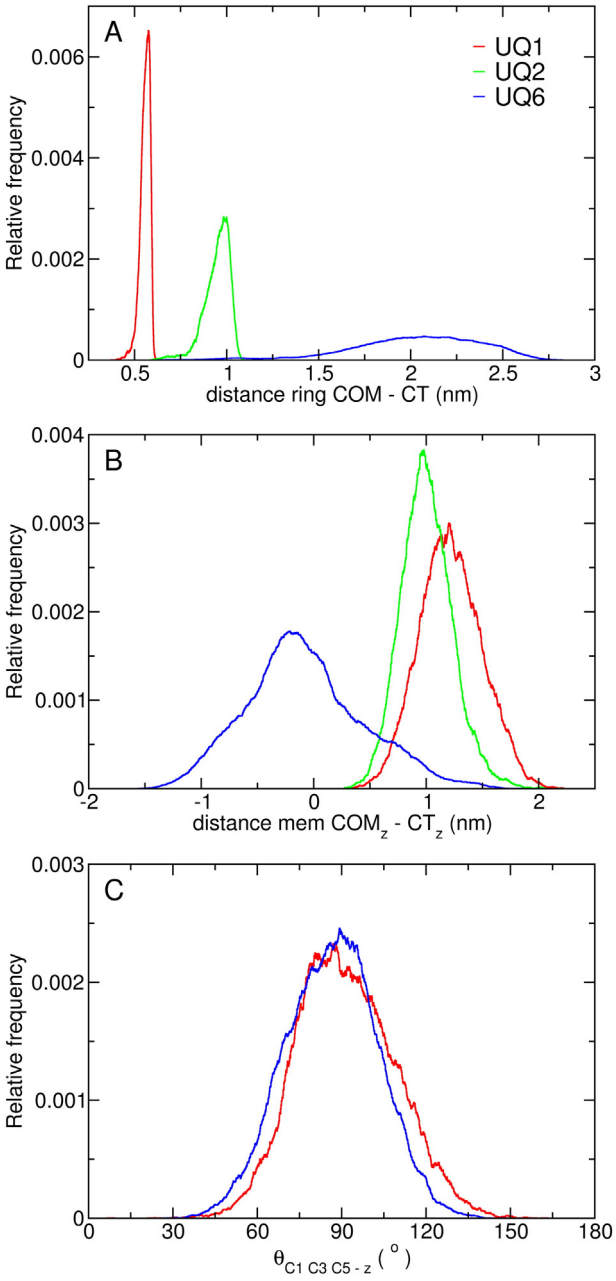

Fig. 7. Ubiquinone localization in the bilayer obtained from unconstrained MD simulations. The distance between ring COM and the last carbon (CT) of ubiquinone isoprenoid tail (panel A), the distance between CT and the membrane COM (B) and the angle between ubiquinone head plane and the membrane midplane (C) for UQ1 (red), UQ2 (green) and UQ6 (blue) are shown. UQ2 curve is not shown in panel C as it is equivalent to UQ1 and would difficult its visualization.

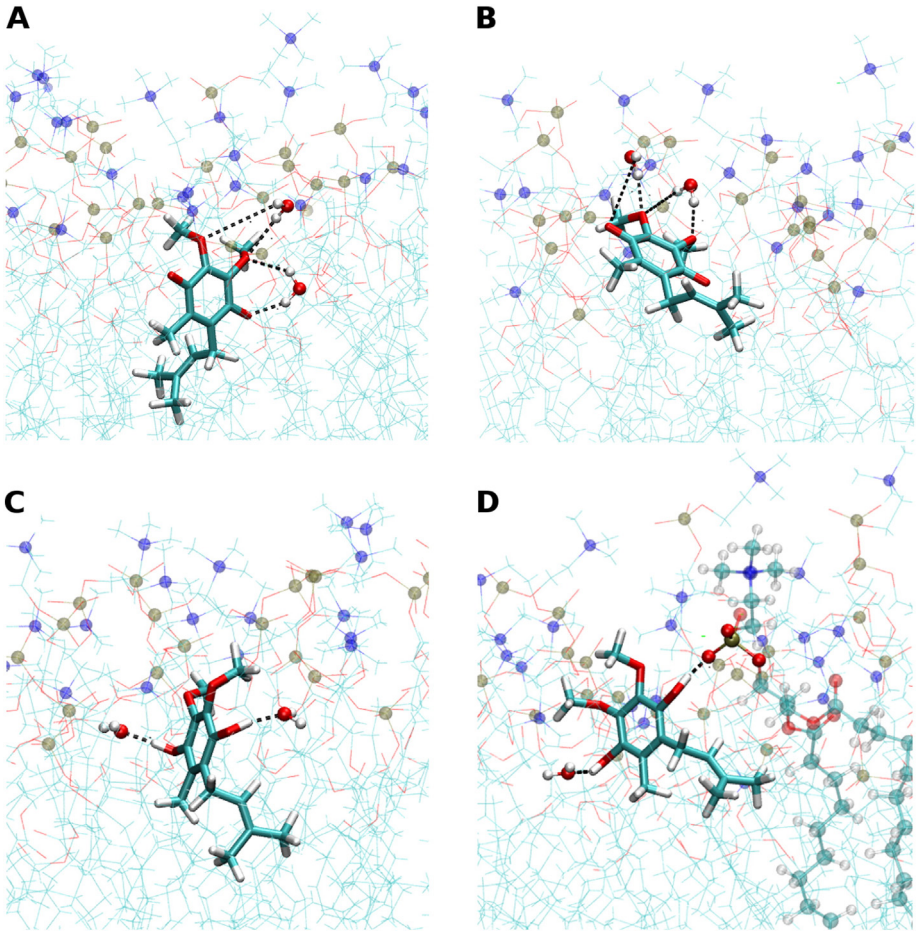

Fig. 8. Selected interactions of ubiquinone with the membrane environment. Ubiquinone is represented in sticks and the lipid bilayer is represented in lines and balls with phosphate P in ochre and choline N in blue. Water molecules and atoms of lipid that interact with UQ1 and UQ1H2 are depicted in balls and sticks, and hydrogen bonds are indicated in black dashed line. Carbon atoms are colored cyan, H in white and O in red. Panels A and B show bidentate water–ubiquinone oxygen hydrogen bonds. Hydrogen bonds of ubiquinol hydrogen with water are show in panel C and with POPC phosphate is shown in panel D.

Considerable effort has been made towards describing ubiquinone localization in lipid bilayers. The two main proposals in the literature suggest that ubiquinone head lies in the bilayer midplane, oriented parallel to membrane plane [6–10] or that the head group is localized near the water–bilayer interface close to the glycerol average position [12–15]. Our results strongly support the second model as the minima observed in all PMFs calculated here corresponds to $z \approx 1.6$ nm. The z insertion coordinate is equivalent to the distance between the membrane midplane and the COM of the ubiquinone head. Thus, contrary to previous suggestions [16], the localization of the ubiquinone head does not change significantly with the length of the isoprenoid tail.

It is remarkable that the average positions of ubiquinone ring in cytochrome bc_1 (complex III) for both the Q_o and Q_i redox sites are observed around the same z-axis values (± 1.6 nm) [68,69]. The entrance of the narrow ubiquinone chamber in NADH:ubiquinone reductase (complex I) is also located near the membrane interface at an approximately similar z-axis value [70]. Thus, the equilibrium location of ubiquinones in a bilayer matches the position of protein binding sites in respiratory complexes, probably facilitating the binding mechanism and increasing the rate of protein binding and unbinding.

The sharp monotonic distribution of the distance between the last isoprenoid carbon (CT) and the COM of the ubiquinone head shown in Fig. 7A for UQ1 and UQ2 suggests a reduced internal flexibility for the tails of ubiquinones with few isoprenoid units. The UQ6 tail, however, has high internal conformational flexibility and a broad distribution centered at 2 nm. A similar broad distribution is observed for the UQ10 terminal isoprenoid carbon (data not shown). The UQ6 tail distribution is altered when ubiquinone is moved inside the membrane (Fig. S4) suggesting that a tail rearrangement is observed during the ubiquinone flip-flop pathway.

Fig. 7B shows the localization of CT regarding membrane normal. The isoprenoid tail is mostly extended and in contact with lipid acyl chains up to about the sixth isoprenoid unit. Given the polar head localization discussed above, ubiquinones span the membrane similar to a POPC molecule. For UQ6 and longer ubiquinones, the tail length is longer than the POPC acyl chain. CT interdigitates over the two bilayer leaflets and it is preferentially localized in the leaflet opposed to its head. For UQ10, the four terminal isoprenoid units have increasingly higher flexibility. In fact, the terminal CT in UQ10 equally samples the whole apolar region of both membrane leaflets (Fig. S4).

This is contrary to previous suggestions that the isoprenoid tail would fold over itself [22,19] and suggests that no aggregation or clustering of ubiquinones inside the lipid bilayer should be observed in the concentration range studied here (~2% per mol) [66]. It should be noted that the distribution of z-axis position of the terminal carbon in POPC (both chains, data not shown) is about an order of magnitude less broad than observed here for ubiquinone CT. The higher flexibility in the ubiquinone tail might be related to its higher diffusion rates (Section 3.4) [19] and may also facilitate binding into the narrow NADH:ubiquinone reductase ubiquinone chamber.

The equilibrium ubiquinone head orientation is indicated in Fig. 7C. For all ubiquinones studied (UQ1 up to UQ10), the quinone head is

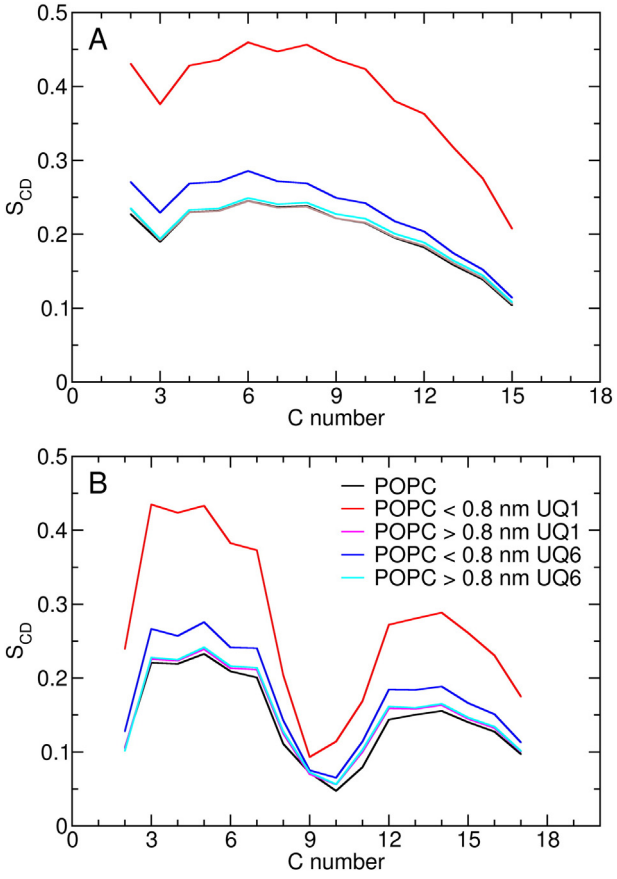

Fig. 9. Calculated carbon-hydrogen bond vector order parameters for POPC sn − 1 (panel A) and for sn-2 (B) acyl chains. Order parameters were calculated for a pure POPC bilayer (black lines) and in the presence of ubiquinone separately for lipid molecules within or further away than 0.8 nm of UQ1 or UQ6 as colored in the legend.

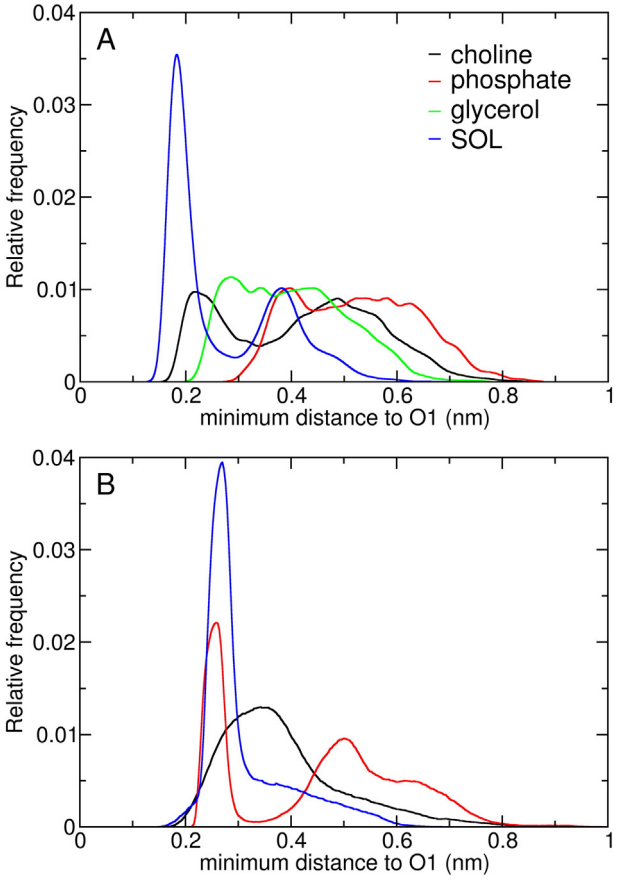

Fig. 10. Minimum distance distribution. Calculations were performed over unconstrained MD simulations between different lipid or solvent groups as shown in the legend and O1 in UQ1 (panel A) and O1 in UQ1H2 (B). SOL is the water solvent.

oriented normal to the membrane, forming an angle of ~90° with the midplane. The angle distribution is rather sharp, with fluctuations smaller than 30° in the time scale of the unconstrained MD simulations. Atoms C5 and C6 of the ubiquinone ring point to the center of the bilayer and atoms C1–C4 point towards the solution phase as expected from the more hydrophilic groups attached to the last centers (Fig. 8). Thus, the ubiquinone orientation when bound to the membrane does not change with increased isoprenoid tail length. When the quinone head is inserted into the low-packing bilayer center (z ~ 0 nm) as well as when it is free in solution (z > 4.0 nm) during the US simulations the whole orientation space is sampled and ubiquinone head tumbles almost freely (Fig. S4).

Since ubiquinones have been suggested to order lipid membranes [9], we have computed carbon–hydrogen order parameters S_{CD} for sn − 1 and sn − 2 chains of POPC for simulations of ubiquinone-free bilayers and for bilayers containing ubiquinones of different isoprenoid chain length. While average S_{CD} order parameters show small shifts for ubiquinone containing bilayers, there was a significant change in order parameters of POPC molecules approximately in the first ubiquinone lipid shell (within 0.7–0.8 nm) as shown in Fig. 9. Acyl chain ordering upon ubiquinone addition observed in fluorescence anisotropy measurements [9] was more pronounced for short tail homologs. This is again in agreement with our simulation results.

Ubiquinone and ubiquinol oxygens were highly hydrated when partitioned into the membrane as shown in Fig. 10. This is due to the interfacial localization of the quinone head and to the bilayer protrusion (Fig. 6). Ubiquinone oxygens, both ketonic and methoxyl (Figs. 10A and S6A) have a first solvation layer formed by water and lipid choline groups. Glycerols have also significant contribution to the first interaction layer, while phosphate groups were farther away. This is again in agreement with previous suggestions from experimental studies [12–15].

Ubiquinol showed a very similar interaction pattern for methoxyl oxygens (Fig. S6B), while hydroxyl oxygens show a perturbed pattern in comparison to the quinone oxygens (Fig. 10B). These hydroxyl oxygens have sharper interactions with the water solvent and with the lipid phosphate group because of the donation of hydrogen bonds. H1 and H4 establish bonds with lipid phosphate groups (Fig. 8D) and water molecules (Fig. 8C) for half of the simulation time. In approximately the other half of the simulation, intramolecular bonds are formed between H1 (H4) and O2 (O3). When located inside the bilayer, the intramolecular hydrogen bonds are prevailing. However, it should be noted that all these hydrogen bonds break and form quickly with an average life time of 1 ns.

The intramolecular hydrogen bonds in UQ1H2 can also be analyzed from the respective C1–O1 (or C4–O4) bond torsions (Fig. 11). The energy minimum of the force-field calculated in vacuum found at ~0° is normally populated in solution as it corresponds to the intramolecular hydrogen bond H1–O2 and H4–O3. The second energy minimum at ±180° is not populated in solution or in the membrane, as water or any H-bond acceptor (such as the lipid phosphate, Fig. 8) is hindered by HM5 or H7 and no hydrogen bond can be established for this configuration. The intermolecular acceptors bind to UQ1H2 hydrogens when this torsion is ±60°, resulting in a broad distribution for C1–O1 (or C4–O4) bond torsions in the [−90°,90°] range.

Rotamers of the methoxide groups with angles of ±70° for torsion of bonds C2–O2 and C3–O3 are more populated in condensed phase than expected from their force-field energy profiles (Fig. 11B). As described

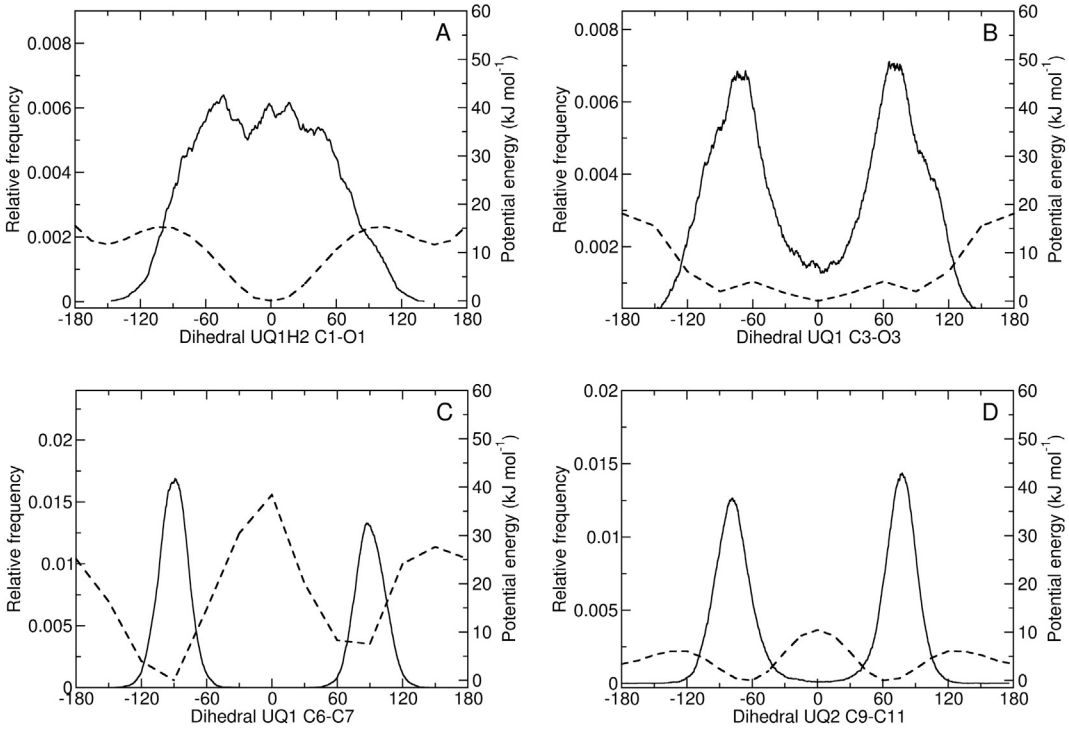

Fig. 11. Dihedral angle distributions of bond torsions. Bond C1–O1 shown in UQ1H2 (panel A), bonds C3–O3 (B) and C6–C7 (C) in UQ1, and bond C9–C11 in UQ2 (D) were calculated over unconstrained MD simulations (full lines). The force-field energy in vacuum is also show in dashed lines.

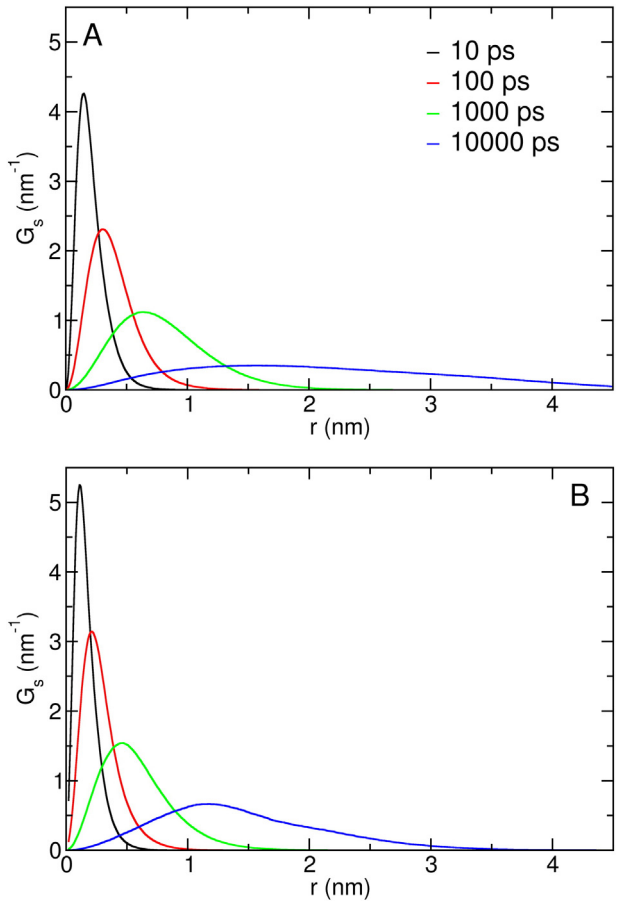

Fig. 12. Self-part of the van Hove correlation function (G_s). Calculations were performed in unconstrained 200 ns MD trajectories for POPC (panel A) and UQ6 (B) at times $t = 0.01$, 0.1, 1, and 10 ns.

above, O2 and O3 are available as H-bond acceptors preferentially for these dihedral angles (Fig. 8A and B) [29]. The region around 0° is less populated as these configurations partially block hydrogen bonding to O1/O4. In the bilayer interior, where no H-bond donors are available, bond torsion distributions are closer to what is expected from the force-field profile (Fig. S5A).

Distributions of non-polar bond torsions are not changed from the corresponding torsion potentials, as shown in Fig. 11C and D for the C6–C7 and C9–C11 bonds in the isoprenoid tail. It should be noted that transitions over the high energy barriers around bond C6–C7 were observed during the unconstrained MD simulation time scale (200 ns).

3.4. Ubiquinone mobility and diffusion over the membrane

The dynamics of ubiquinone embedded in the bilayer was investigated by the self part of van Hove correlation function, $G_s(r, \Delta t)$ [71,72]. This function gives the probability for a particle to show position displacements (r) in Δt time intervals. The van Hove distributions for POPC at 0.01 ns and longer times are gaussian-shaped as shown in Fig. 12. This is expected for a simple diffusion mechanism and is in agreement with a fast characteristic relaxation time (<10 ps) for lipids

Table 2
Experimental and simulated (MD) lateral diffusion coefficients (in 10^{-7} cm^2 s^{-1}) for various ubiquinones complexed to lipid bilayers.[a]

	Experiment	MD
UQ1	6[19], 9[14]	4.2
UQ1H2		12.0
UQ2	12[19], 25[14]	4.0
UQ6		4.7
UQ10	13[19], 2.6[20], 5[14]	5.3
POPC	1.5[76]	6.0

[a] Experimental coefficients were measured by fluorescence quenching in asolectin vesicles [19,14,20] and by NMR relaxation in pure POPC oriented bilayers [76] in temperatures of ~310 K. Simulated values were obtained from the angular coefficient of the linear region of Eq. (3) calculated from unconstrained MD simulations.

in liquid crystalline phase [73,74]. In this regime, the mean square displacement has a linear dependence with respect to time ($x^2(t) \propto t$). The same behavior is observed for ubiquinone and ubiquinol, but relaxation times are shorter and higher displacements are observed in the same timescale.

In contrast to what is observed for the pure POPC lipid, linearity of squared-displacement $x^2(t)$ with time is lost for ubiquinones at times longer than 25 ns, already observed from the non-gaussian shape of the $t = 10$ ns curve for UQ6 (Fig. 12B). It may be attributed to a slow relaxation process of the lipid polar group and water solvating ubiquinone at the bilayer interface.

Table 2 shows lateral diffusion coefficients D calculated from the Einstein relation:

$$D = \lim_{t \to \infty} \frac{\langle x^2(t) \rangle}{4t}. \quad (4)$$

Similar values (not shown) were calculated from fitting the self part of van Hove correlation function to a gaussian function (whereas $G_s(r, \Delta t) = (r/2D\Delta t)\exp[-r^2/4D\Delta t]$) [75].

Calculated lateral diffusion constants are about the same for all ubiquinones (UQ1–UQ10). But, diffusion is three times faster for ubiquinol (UQ1H2). The value calculated for POPC diffusion is in between. This result suggests that the polar region in amphipathic molecules is the major determinant of their diffusion dynamics. The calculated results should be compared to diffusion coefficients obtained from experiments that probe similar molecular scales. Thus, given the simulated time (ns) and length (nm) scales, methods such as fluorescence collisional quenching and NMR relaxation are the most appropriate for comparisons [22,19]. As shown in Table 2, these methods give experimental diffusion constants that vary up to one order of magnitude (2.6–25 10^{-7} cm^2 s^{-1}) for different ubiquinones and membrane preparations. Results from other methods such as fluorescence recovery after photo-bleaching probe rather different length scales (μm) and yield slower diffusion constants in the order of 10^{-8} to 10^{-9} cm^2 s^{-1}[17, 21]. Thus, we conclude that results for the calculated diffusion constants are in the same order of magnitude to experimental measurements for both POPC pure lipid bilayers [76] and for ubiquinone embedded in the bilayer [18].

4. Conclusions

An accurate energy model of ubiquinone is crucial to describe its conformational flexibility and interfacial behavior. Here, we have parametrized a CHARMM compatible force-field for ubiquinone with special attention to group polarity and torsional barriers involving the isoprenoid tail. The description of water interactions with the ubiquinone polar head was also significantly improved. The proposed force-field and simulation model were validated against experimental data and important insight on the ubiquinone interfacial behavior was obtained by computing free energies for a series of homologs. The convergence of PMFs for long amphiphiles such as ubiquinones interacting with lipid bilayers was tackled by two enhanced sampling methods, umbrella sampling and bias-exchange metadynamics.

We performed a detailed analysis of ubiquinone interaction within the lipid bilayer by addressing structural and dynamical properties. Results are in line with previous experimental studies [11–15] and support the proposal that ubiquinone head is localized in the interfacial region near the lipid glycerol groups and is highly hydrated due to membrane protrusion. The head plane displays a normal orientation with respect to the membrane midplane direction. Isoprenyl tails are extended and packed with the lipid acyl chains. In long tail homologs such as UQ6 and UQ10, the isoprenoid chain interdigitates across the bilayer and its terminal isoprenoid units have high flexibility. The internal torsions of ubiquinone are modulated by the condensed phase. In particular, ubiquinol hydrogen bonds to the lipid phosphate group, to water and intermolecularly to its methoxide oxygens. It was also found that the diffusion rate of various ubiquinones embedded in a bilayer is similar to that of POPC lipids.

Notably the equilibrium position of ubiquinone head along the bilayer normal z-axis is coincident with the modulus of the average position of ubiquinone redox sites in cytochrome bc_1 and with the entrance of the binding site in NADH:ubiquinone reductase. Given the rather small changes observed here for polar head localization and orientation, and dynamics for ubiquinones with different isoprenoid tail lengths, we can also speculate that, in the complex lipid mixtures observed in bacterial or mitochondrial membranes — which lack cholesterol in their content, changes in bilayer acyl lipid composition will result in small perturbations to the ubiquinone partition and dynamics observed here.

The energy model and molecular dynamics simulations presented here for several ubiquinone homologs provide important insights on their behavior when embedded in a lipid bilayer. These results constitute a benchmark to studies of the transport and complexation mechanisms of this universal charge carrier with proteins involved in cellular respiration and photosynthesis.

Transparency document

The Transparency document associated with this article can be found, in the online version.

Acknowledgments

Funding from FAPESP (projects 12/02501-4, 12/17833-2 and 14/21900-2) is acknowledged.

Appendix A. Supplementary data

Supplementary data to this article can be found online at http://dx.doi.org/10.1016/j.bbabio.2015.08.001.

References

[1] P. Mitchell, Coupling of phosphorylation to electron and hydrogen transfer by a chemi-osmotic type of mechanism, Nature 191 (4784) (1961) 144–148.
[2] D. Green, The mitochondrial electron transfer system, Comp. Biochem. 14 (1966) 309–326.
[3] A. Kröger, M. Klingenberg, S. Schweidler, Further evidence for the pool function of ubiquinone as derived from the inhibition of the electron transport by antimycin, Eur. J. Biochem. 39 (2) (1973) 313–323.
[4] C. Heron, C. Ragan, B. Trumpower, The interaction between mitochondrial NADH-ubiquinone oxidoreductase and ubiquinol-cytochrome c oxidoreductase. restoration of ubiquinone-pool behaviour, Biochem. J. 174 (1978) 791–800.
[5] L. Ernster, G. Dallner, Biochemical, physiological and medical aspects of ubiquinone function, Biochim. Biophys. Acta (BBA) - Mol. Basis Dis. 1271 (1) (1995) 195–204.
[6] H. Katsikas, P. Quinn, The polyisoprenoid chain length influences the interaction of ubiquinones with phospholipid bilayers, Biochim. Biophys. Acta 689 (1982) 363–369.
[7] H. Katsikas, P.J. Quinn, Fluorescence probe studies of the distribution of ubiquinone homologues in bilayers of dipalmitoylglycerophosphocholine, Eur. J. Biochem. 131 (1983) 607–612.
[8] G. Metz, K. Howard, W. van Liemt, J. Prestegard, J. Lugtenburg, S. Smith, NMR studies of ubiquinone location in oriented model membranes: evidence for a single motionally-averaged population, J. Am. Chem. Soc. 117 (1995) 564–565.
[9] M. Jemiola-Rzeminska, J. Kruk, M. Skowronek, K. Strzalka, Location of ubiquinone homologues in liposome membranes studied by fluorescence anisotropy of diphenyl-hexatriene and trimethylammonium-diphenyl-hexatriene, Chem. Phys. Lipids 79 (1996) 55–63.
[10] T. Hauß, S. Dante, T.H. Haines, N.A. Dencher, Localization of coenzyme Q10 in the center of a deuterated lipid membrane by neutron diffraction, Biochim. Biophys. Acta 1710 (2005) 57–62.
[11] P.B. Kingsley, G.W. Feigenson, 1 H-NMR study of the location and motion of ubiquinones in perdeuterated phosphatidylcholine bilayers, Biochim. Biophys. Acta Bioenerg. 635 (3) (1981) 602–618.
[12] M.A. Stidham, T. McIntosh, J.N. Siedow, On the localization of ubiquinone in phosphatidylcholine bilayers, Biochim. Biophys. Acta 767 (1984) 423–431.
[13] B.A. Cornell, M.A. Keniry, A. Post, R.N. Robertson, L.E. Weir, P.W. Westerman, Location and activity of ubiquinone 10 and ubiquinone analogues in model and biological membranes, Biochemistry 26 (24) (1987) 7702–7707.

[14] G. Lenaz, B. Samori, R. Fato, M. Battino, G.P. Castelli, I. Domini, Localization and preferred orientations of ubiquinone homologs in model bilayers, Biochem. Cell Biol. 70 (1992) 504–514.
[15] M. Afri, B. Ehrenberg, Y. Talmon, J. Schmidt, Y. Cohena, A.A. Frimer, Location and mobility of ubiquinones of different chain lengths in artificial membrane vesicles, Chem. Phys. Lipids 131 (2004) 107–121.
[16] G. Lenaz, Quinone specificity of complex I, Biochim. Biophys. Acta 1364 (1998) 207–221.
[17] S. Gupte, E.-S. Wu, L. Hoechli, M. Hoechli, K. Jacobson, A.E. Sowers, C.R. Hackenbrock, Relationship between lateral diffusion, collision frequency, and electron transfer of mitochondrial inner membrane oxidation–reduction components, Proc. Natl. Acad. Sci. U. S. A. 81 (1984) 2606–2610.
[18] R. Fato, M. Battino, M.D. Esposti, G.P. Castelli, G. Lenaz, Determination of partition and lateral diffusion coefficients of ubiquinones by fluorescence quenching of n-(9-Anthroy1oxy)stearic acids in phospholipid vesicles and mitochondrial membranes, Biochemistry 25 (1986) 3378–3390.
[19] S.D. Bernardo, R. Fato, R. Casadio, P. Fariselli, G. Lenaz, A high diffusion coefficient for coenzyme Q10 might be related to a folded structure, FEBS Lett. 426 (1998) 77–80.
[20] R. Fato, E. Estornell, S.D. Bernardo, F. Pallotti, G.P. Castelli, G. Lenaz, A method for estimating lateral diffusion coefficients in membranes from steady-state fluorescence quenching studies, Biophys. J. 51 (1987) 735–744.
[21] I. Llorente-Garcia, T. Lennc, H. Erhardt, O.L. Harriman, L.-N. Liu, A. Robson, S.-W. Chiu, S. Matthews, N.J. Willis, C.D. Bray, S.-H. Lee, J.Y. Shin, C. Bustamante, J. Liphardt, T. Friedriche, C.W. Mullineaux, M.C. Leak, Single-molecule in vivo imaging of bacterial respiratory complexes indicates delocalized oxidative phosphorylation, Biochim. Biophys. Acta 1837 (2014) 811–824.
[22] J.A. Söderhäll, A. Laaksonen, Molecular dynamics simulations of ubiquinone inside a lipid bilayer, J. Phys. Chem. B 105 (2001) 9308–9315.
[23] H.A. Filipe, M.J. Moreno, T. Róg, I. Vattulainen, L.M. Loura, How to tackle the issues in free energy simulations of long amphiphiles interacting with lipid membranes: convergence and local membrane deformations, J. Phys. Chem. B 118 (2014) 3572–3581.
[24] Z. Ghaemi, M. Minozzi, P. Carloni, A. Laio, A novel approach to the investigation of passive molecular permeation through lipid bilayers from atomistic simulations, J. Phys. Chem. B 116 (2012) 8714–8721.
[25] J.P. Jambeck, A.P. Lyubartsev, Exploring the free energy landscape of solutes embedded in lipid bilayers, J. Phys. Chem. Lett. 4 (2013) 1781–1787.
[26] F. Autenrieth, E. Tajkhorshid, J. Baudry, Z. Luthey-Schulten, Classical force field parameters for the heme prosthetic group of cytochrome c, J. Comput. Chem. 25 (13) (2004) 1613–1622.
[27] A. Aird, J. Wrachtrup, K. Schulten, C. Tietz, Possible pathway for ubiquinone shuttling in *Rhodospirillum rubrum* revealed by molecular dynamics simulations, Biophys. J. 92 (1) (2007) 23–33.
[28] K. Kaszuba, P.A. Postila, O. Cramariuc, M. Sarewicz, A. Osyczka, I. Vattulainen, T. Róg, Parametrization of the prostetic redox centers of the bacterial cytochrome Bc1 complex for atomistic molecular dynamics simulations, Theor. Chem. Accounts 132 (1370) (2013) 1–11.
[29] J.V. Vermaas, A.T. Taguchi, S.A. Dikanov, C.A. Wraight, E. Tajkhorshid, Redox potential tuning through differential quinone binding in the photosynthetic reaction center of *Rhodobacter sphaeroides*, Biochemistry 54 (2015) 2104–2116.
[30] J.A. Nilsson, A. Lyubartsev, L.A. Eriksson, A. Laaksonen, Molecular dynamics simulations of ubiquinone; a survey over torsional potentials and hydrogen bonds, Mol. Phys. 99 (21) (2001) 1795–1804.
[31] A.D. MacKerell Jr., D. Bashford, M. Bellott, R.L. Dunbrack Jr., J.D. Evanseck, M.J. Field, S. Fischer, J. Gao, H. Guo, S. Ha, D. Joseph-McCarthy, L. Kuchnir, K. Kuczera, F.T.K. Lau, C. Mattos, S. Michnick, T. Ngo, D.T. Nguyen, B. Prodhom, W. E. R. III, B. Roux, M. Schlenkrich, J.C. Smith, R. Stote, J. Straub, M. Watanabe, J. Wirkiewicz-Kuczera, D. Yin, M. Karplus, All-atom empirical potential for molecular modeling and dynamics studies of proteins, J. Phys. Chem. B 102 (1998) 3586–3616.
[32] K. Vanommeslaeghe, E. Hatcher, C. Acharya, S. Kundu, S. Zhong, J. Shim, E. Darian, O. Guvench, P. Lopes, I. Vorobyov, A. D. M. Jr., CHARMM General Force Field: a force field for drug-like molecules compatible with the CHARMM all-atom additive biological force fields, J. Comput. Chem. 31 (4) (2010) 671–690.
[33] J.B. Klauda, R.M. Venable, J.A. Freites, J.W. O'Connor, D.J. Tobias, C. Mondragon-Ramirez, I. Vorobyov, A. D. M. Jr., R.W. Pastor, Update of the CHARMM all-atom additive force field for lipids: validation on six lipid types, J. Phys. Chem. B 114 (23) (2010) 7830–7843.
[34] P. Hratchian, A.F. Izmaylov, J. Bloino, G. Zheng, J.L. Sonnenberg, M. Hada, M. Ehara, K. Toyota, R. Fukuda, J. Hasegawa, M. Ishida, T. Nakajima, Y. Honda, O. Kitao, H. Nakai, T. Vreven, J.A. Montgomery Jr., J.E. Peralta, F. Ogliaro, M. Bearpark, J.J. Heyd, E. Brothers, K.N. Kudin, V.N. Staroverov, R. Kobayashi, J. Normand, K. Raghavachari, A. Rendell, J.C. Burant, S.S. Iyengar, J. Tomasi, M. Cossi, N. Rega, J.M. Millam, M. Klene, J.E. Knox, J.B. Cross, V. Bakken, C. Adamo, J. Jaramillo, R. Gomperts, R.E. Stratmann, O. Yazyev, A.J. Austin, R. Cammi, C. Pomelli, J.W. Ochterski, R.L. Martin, K. Morokuma, V.G. Zakrzewski, G.A. Voth, P. Salvador, J.J. Dannenberg, S. Dapprich, A.D. Daniels, Farkas, J.B. Foresman, J.V. Ortiz, J. Cioslowski, D.J. Fox, Gaussian 09, Revision A.1, Gaussian, Inc., Wallingford CT, 2009.
[35] A.D. Becke, A new mixing of Hartree–Fock and local density-functional theories, J. Chem. Phys. 98 (2) (1993) 1372–1377.
[36] W.J. Hehre, R. Ditchfield, J.A. Pople, Selfconsistent molecular orbital methods. XII. Further extensions of GaussianType basis sets for use in molecular orbital studies of organic molecules, J. Chem. Phys. 56 (5) (1972) 2257–2261.
[37] A. Szabo, N. Ostlund, Modern Quantum Chemistry, 1st edn Dover, New York, 1989.
[38] F.B. Van Duijneveldt, J.G.C.M. Van de Rijdt, J.H. Van Lenthe, State of the art in counterpoise theory, Chem. Rev. 94 (1994) 1873–1885.
[39] W.L. Jorgensen, J. Chandrasekhar, J.D. Madura, R.W. Impey, M.L. Klein, Comparison of simple potential functions for simulating liquid water, J. Chem. Phys. 79 (1983) 926–935.
[40] S. Pronk, S. Pall, R. Schulz, P. Larsson, P. Bjelkmar, R. Apostolov, M.R. Shirts, J.C. Smith, P.M. Kasson, D. van der Spoel, B. Hess, E. Lindahl, GROMACS 4.5: a high-throughput and highly parallel open source molecular simulation toolkit, Bioinformatics 29 (2013) 845–854, http://dx.doi.org/10.1093/bioinformatics/btt055.
[41] G.M. Arantes, M. Loos, Specific parametrisation of a hybrid potential to simulate reactions in Phosphatases, Phys. Chem. Chem. Phys. 8 (2006) 347–353.
[42] G. Bussi, D. Donadio, M. Parrinello, Canonical sampling through velocity rescaling, J. Chem. Phys. 126 (014101) (2007) 1–7.
[43] H. Berendsen, J. Postma, W. vanGunsteren, A. DiNola, J. Haak, Molecular dynamics with coupling to an external bath, J. Chem. Phys. 81 (8) (1984) 3684–3690.
[44] T. Darden, D. York, L. Pedersen, Particle Mesh Ewald: an N-log(N) method for Ewald sums in large systems, J. Chem. Phys. 98 (12) (1993) 10089–10092.
[45] B. Hess, H. Bekker, H.J. Berendsen, J.G. Fraaije, LINCS: a linear constraint solver for molecular simulations, J. Comput. Chem. 18 (12) (1997) 1463–1472.
[46] C. Anézo, A.H. de Vries, H.-D. Höltje, D.P. Tieleman, S.-J. Marrink, Methodological issues in lipid bilayer simulations, J. Phys. Chem. B 107 (2003) 9424–9433.
[47] N. Kucerka, S. Tristram-Nagle, J.F. Nagle, Structure of fully hydrated fluid phase lipid bilayers with monounsaturated chains, J. Mol. Biol. 208 (3) (2005) 193–202.
[48] M. Javanainen, Universal method for embedding proteins into complex lipid bilayers for molecular dynamics simulations, J. Chem. Theory Comput. 10 (2014) 2577–2582.
[49] A. Einstein, Investigations on the Theory of the Brownian Movement, Courier Corporation, 1956.
[50] T.D. Romo, N. Leioatts, A. Grossfield, Lightweight object oriented structure analysis: tools for building tools to analyze molecular dynamics simulations, J. Comput. Chem. 35 (32) (2014) 2305–2318.
[51] G. Torrie, J. Valleau, Nonphysical sampling distributions in Monte Carlo free-energy estimation: umbrella sampling, J. Comp. Physiol. 23 (2) (1977) 187–199.
[52] S. Piana, A. Laio, A bias-exchange approach to protein folding, J. Phys. Chem. B 111 (17) (2007) 4553–4559.
[53] S. Kumar, J.M. Rosenberg, D.B.R.H. Swendsen, P.A. Kollman, The weighted histogram analysis method for free-energy calculations on biomolecules. I. The method, J. Comput. Chem. 13 (8) (1992) 1011–1021.
[54] J.S. Hub, B.L. de Groot, D. van der Spoel, g_wham—A free weighted histogram analysis implementation including robust error and autocorrelation estimates, J. Chem. Theory Comput. 6 (12) (2010) 3713–3720.
[55] A. Laio, M. Parrinello, Escaping free-energy minima, Proc. Natl. Acad. Sci. U. S. A. 99 (20) (2002) 12562–12566.
[56] M. Bonomi, D. Branduardi, G. Bussi, C. Camilloni, D. Provasi, P. Raiteri, D. Donadio, F. Marinelli, F. Pietrucci, R.A. Broglia, M. Parrinello, PLUMED: a portable plugin for free-energy calculations with molecular dynamics, Comput. Phys. Commun. 180 (2009) 1961–1972.
[57] A. Laio, F.L. Gervasio, Metadynamics: a method to simulate rare events and reconstruct the free energy in biophysics, chemistry and material science, Rep. Prog. Phys. 71 (126601) (2008) 1–22.
[58] Y. Crespo, A. Laio, G.E. Santoro, E. Tosatti, Calculating thermodynamics properties of quantum systems by a non-Markovian Monte Carlo procedure, Phys. Rev. E 80 (015702) (2009) 1–4.
[59] I.J. General, A note on the standard states binding free energy, J. Chem. Theory Comput. 6 (8) (2010) 2520–2524.
[60] H. Ku, Notes on the use of propagation of error formulas, J. Res. Natl. Bur. Stand. 70 (4) (1966) 263–273.
[61] C. Neale, W.D. Bennett, D.P. Tieleman, R. Pomès, Statistical convergence of equilibrium properties in simulations of molecular solutes embedded in lipid bilayers, J. Chem. Theory Comput. 7 (2011) 4175–4188.
[62] C. Neale, C. Madill, S. Rauscher, R. Pomès, Accelerating convergence in molecular dynamics simulations of solutes in lipid membranes by conducting a random walk along the bilayer normal, J. Chem. Theory Comput. 9 (8) (2013) 3686–3703.
[63] M.J. Hinner, S.-J. Marrink, Alex H. de Vries, Location, tilt, and binding: a molecular dynamics study of voltage-sensitive dyes in biomembranes, J. Phys. Chem. B 113 (48) (2009) 15807–15819.
[64] V.E. Kagan, E.A. Serbinova, G.M. Koynova, S.A. Kitanova, V.A. Tyurin, T.S. Stoytchev, P.J. Quinn, L. Packer, Antioxidant action of ubiquinol homologues with different isoprenoid chain length in biomembranes, Free Radic. Biol. Med. 9 (1990) 117–126.
[65] J.A. Platts, M.H. Abraham, D. Butina, A. Hersey, Estimation of molecular linear free energy relationship descriptors by a group contribution approach. 2. Prediction of partition coefficients, J. Chem. Inf. Comput. Sci. 40 (1) (2000) 71–80.
[66] R. Fato, E. Estornell, S.D. Bernardo, F. Pallotti, G.P. Castelli, G. Lenaz, Steady-state kinetics of the reduction of coenzyme Q analogs by complex I (NADH:ubiquinone oxidoreductase) in bovine heart mitochondria and submitochondrial particles, Biochemistry 35 (1996) 2705–2716.
[67] R. Fato, C. Castelluccio, G. Palmer, G. Lenaz, A simple method for the determination of the kinetic constants of membrane enzymes utilizing hydrophobic substrates: ubiquinol cytochrome c reductase, Biochim. Biophys. Acta 932 (1988) 216–222.
[68] S. Iwata, J.W. Lee, K. Okada, J.K. Lee, M. Iwata, B. Rasmussen, T.A. Link, S. Ramaswamy, B. Jap, Complete structure of the 11-subunit bovine mitochondrial cytochrome bc1 complex, Science 281 (1998) 64–71.
[69] C. Lange, J.H. Nett, B.L. Trumpower, C. Hunte, Specific roles of protein–phospholipid interactions in the yeast cytochrome bc_1 complex structure, EMBO J. 20 (2001) 6591–6600.
[70] R. Baradaran, J.M. Berrisford, G.S. Minhas, L.A. Sazanov, Crystal structure of the entire respiratory complex I, Nature 494 (2013) 443–448.

[71] L. van Hove, Correlations in space and time and born approximation scattering in systems of interacting particles, Phys. Rev. 95 (1) (1954) 249–3720.
[72] M.P. Allen, D.J. Tildesley, J.R. Banavar, Computer Simulation of Liquids, vol. 42, American Institute of Physics, 2008.
[73] P. Khalatur, N. Balabaev, A. Pavlov, Molecular dynamics study of a lipid bilayer and a polymer liquid, Mol. Phys. 59 (4) (1986) 753–773.
[74] F.W. Starr, B. Hartmanna, J.F. Douglas, Dynamical clustering and a mechanism for raft-like structures in a model lipid membrane, Soft Matter 10 (2014) 3036–3047.
[75] P.S. Niemela, M.S. Miettinen, L. Monticelli, H. Hammaren, P. Bjelkmar, T. Murtola, E. Lindahl, I. Vattulainen, Membrane proteins diffuse as dynamic complexes with lipids, J. Am. Chem. Soc. 132 (22) (2010) 7574–7575.
[76] A. Filippov, G. Orodd, G. Lindblom, Influence of cholesterol and water content on phospholipid lateral diffusion in bilayers, Langmuir 19 (2003) 6397–6400.